AMERICAN ACADEMY OF OPHTHALMOLOGY®

Vision-Threatening Diabetic Macular Ischemia Based on Inferred Progression Pathways in OCT Angiography

Miyo Yoshida, MD, Tomoaki Murakami, MD, PhD, Keiichi Nishikawa, MD, Kenji Ishihara, MD, PhD, Yuki Mori, MD, PhD, Akitaka Tsujikawa, MD, PhD

Purpose: To elucidate the progression pathways of diabetic macular ischemia (DMI) using OCT angiography (OCTA) images and to assess changes in visual acuity (VA) associated with each pathway.

Design: A single-center, prospective case series study.

Participants: One hundred fifty-one eyes from 151 patients with a 3-year follow-up period.

Methods: We obtained 3 × 3 mm swept-source OCTA images and conducted analyses of en face images within a central 2.5 mm diameter circle. Nonperfusion squares (NPSs) were defined as 15 × 15-pixel squares without retinal vessels. Each eye at baseline and after 3 years was embedded into a 2-dimensional uniform manifold approximation and projection space and assigned to 1 of 5 severity grades—*Initial*, *Mild*, *Superficial*, *Moderate*, and *Severe*—using the k-nearest neighbors method. We assessed major transitions (involving ≥4 cases) during 3 years. Subsequent probabilistic analyses enabled the construction of a graphical model, wherein directed arrows represented inferred pathways of DMI progression. From this cohort, 103 eyes of 103 patients who did not receive any ocular treatments during the follow-up period were subsequently evaluated for VA changes.

Main Outcome Measures: Inference of DMI progression pathways.

Results: In most cases, NPS counts increased in both the superficial and deep layers. The major transitions between these severity groups at 3 years displayed a unique distribution, and probabilistic analyses suggested a directed graphical model comprising 7 inferred pathways of DMI progression: *Initial* to *Mild*, *Initial* to *Superficial*, *Mild* to *Superficial*, *Mild* to *Moderate*, *Superficial* to *Moderate*, *Superficial* to *Severe*, and *Moderate* to *Severe.* Eyes of the *Mild* and *Superficial* groups had greater increases in superficial NPS within the central sector than those of the *Severe* group. Additionally, deep NPS counts within the central sector decreased more in the eyes of the *Initial* group than in those of the *Superficial* and *Moderate* groups. Notably, the eyes of the *Superficial* and *Moderate* groups exhibited greater VA deterioration at 3 years compared with those in the *Initial* group.

Conclusions: A directed graphical model of DMI progression may serve as a useful tool for inferring progression pathways and predicting VA deterioration.

Financial Disclosure(s): Proprietary or commercial disclosure may be found in the Footnotes and Disclosures at the end of this article. *Ophthalmology Science 2025;5:100761 © 2025 by the American Academy of Ophthalmology. This is an open access article under the CC BY-NC-ND license (http://creativecommons.org/licenses/by-nc-nd/4.0/).*

Supplemental material available at www.ophthalmologyscience.org.

In the era of anti-VEGF treatment, diabetic macular ischemia (DMI) is the third vision-threatening diabetic retinopathy (DR), and effective therapeutic strategies should be established.[1,2] Capillary nonperfusion reduces the supply of oxygen and nutrients, subsequently leading to visual acuity (VA) reduction and poor retinal sensitivity.[3–11] In addition, retinal ischemia is associated with 2 major pathological mechanisms: retinal edema and neurodegeneration.[1,12–14] Hypoxia-induced VEGF expression increases vascular hyperpermeability and plays a pivotal role in the pathogenesis of diabetic macular edema.[15,16] On the other hand, nonperfusion areas (NPAs) are accompanied by disorganization of retinal inner layers and disruption of the ellipsoid zone of photoreceptors on spectral-domain OCT images, which may represent layer-by-layer degenerative processes and resultant irreversible visual dysfunction.[14,17]

Advances in fundus imaging are providing new insights into capillary nonperfusion. Retinal vessels in the macula reside in the ganglion cell layer and bifurcate into 2 capillary layers at the inner and outer boundaries of the inner nuclear layer.[18,19] A classic modality, fluorescein angiography, can delineate the foveal avascular zone (FAZ) but cannot visualize layer-by-layer capillaries in the parafovea.[20] In contrast, OCT angiography (OCTA) images with higher contrast have enabled the assessment of 3-dimensional vascular structures and the quantification of vascular parameters.[2,6,9,20–22] Automatic measurement of perfusion and nonperfusion metrics on OCTA images has improved the assessment of DMI severity compared with traditional

https://doi.org/10.1016/j.xops.2025.100761
ISSN 2666-9145/25

FAZ parameters on fluorescein angiography images.[1] A recent publication has proposed a novel severity scale of DMI based on the distribution as well as the amounts of NPAs on OCTA images.[23] However, the gold standard for DMI diagnosis or grading remains to be determined.

Despite its clinical relevance, the processes of DMI progression remain poorly understood. In most cases, capillary nonperfusion exacerbates irreversibly, highlighting the importance of both preventive and therapeutic strategies for DMI. Vascular morphologies on OCTA images demonstrate a continuum from healthy intercapillary spaces to NPAs in eyes with DR.[24] On the other hand, we often observe unique patterns of capillary nonperfusion in eyes with DMI, e.g., FAZ enlargement, capillary dropout in the temporal subfield, and nonperfusion predominantly in the deep layer.[25] This suggests that the clinical characterization of DMI progression sheds light on the neurovascular degeneration in DMI.

In this study, we investigated the progression pathways of DMI on OCTA images and the VA deterioration in each pathway after 3 years.

Methods

Participants

In this prospective study, 162 consecutive eyes of 162 patients with DR were initially enrolled at the Department of Ophthalmology in Kyoto University Hospital between July 2017 and December 2020. However, 11 patients were lost to follow-up over the 3-year period, resulting in a final cohort of 151 eyes. This cohort is completely independent of our previous study.[23] Among them, 103 eyes that received no ocular treatment during the follow-up period were included in the analysis of VA changes. This subgroup comprised both treatment-naïve and previously treated cases. This study was approved by the Kyoto University Graduate School and Faculty of Medicine Ethics Committee and adhered to the tenets of the Declaration of Helsinki. Written informed consent was obtained from all participants before inclusion in the study.

We evaluated eyes with DR for which swept-source OCTA (SS-OCTA) images of sufficient quality (signal strength index of $\geq$8) were acquired. The inclusion criteria were the presence of DR, the acquisition of 3 $\times$ 3 mm SS-OCTA images centered on the fovea at baseline and at the 3-year visit, and written informed consent. Exclusion criteria were severe media opacity, other ocular diseases that lead to visual impairment, an axial length of $<$22 mm or $>$26 mm, any other chorioretinal disease, including epiretinal membrane and vitreomacular traction, glaucoma, previous treatment within 6 months before imaging (e.g., anti-VEGF injection, ocular steroids, intraocular surgery, or photocoagulation), and vitrectomy with macular interventions such as membrane peeling during the follow-up period. For VA subgroup analyses, eyes that received any ocular treatment during the follow-up period were excluded. Additional exclusion criteria were severe segmentation error in the superficial slab or poor image quality (signal strength index $\leq$7). If both eyes met these criteria, the right eye was selected for this study.

Image Acquisition and Processing

After measurement of best-corrected decimal VA using a full protocol refraction and its conversion to the logarithm of the minimum angle of resolution (logMAR) VA, comprehensive ophthalmic examinations were performed, including assessment of DR severity based on the International Clinical Diabetic Retinopathy Severity Scales.[26] Central subfield thickness and axial length were measured using Spectralis OCT (Heidelberg Engineering) and partial coherence interferometry (IOL Master, Carl Zeiss Meditec, Inc), respectively. Eyes with a central subfield thickness of $>$305 μm or 320 μm for female or male patients, respectively, were diagnosed as center-involved diabetic macular edema.[27]

We acquired SS-OCTA images within the nominal 3 $\times$ 3 mm square centered on the fovea using Plex Elite 9000 (Carl Zeiss Meditec, Inc). The images of the left eye were horizontally inverted to standardize the nasal subfield positioning. The en face OCTA images with 300 $\times$ 300 A-scans were digitally converted to a 1024 $\times$ 1024 pixel array for quantitative analyses. The en face images in the superficial layer (from the inner limiting membrane to the boundary of the inner plexiform layer and inner nuclear layer) were created based on the default setting of the installed software. The deep en face images (from the inner border of the inner nuclear layer to 70 μm above the retinal pigment epithelium) were prepared based on the custom setting of the same software, as described previously.[28]

We semiautomatically determined the amounts and locations of NPAs on SS-OCTA images as described previously.[23] Briefly, the edges of retinal vessels were automatically detected, utilizing the Canny Edge Detector plugin of ImageJ software (National Institutes of Health, http://imagej.nih.gov/ij/).[29] The 2.5 mm circle was divided into 15 $\times$ 15 pixel squares, and the square with no signals of vascular edges was defined as nonperfusion squares (NPSs). To explore the distribution of capillary nonperfusion, we counted the NPSs in 5 sectors, i.e., the central (1-mm area) and 4 parafoveal (1−2.5 mm) subfields (nasal, superior, temporal, and inferior) of the ETDRS grid.

Inference of Progression Pathways

We employed 4 steps of data analysis of high-dimensional data in order to explore the progression pathways of DMI: (1) embedding of each case onto 2-dimensional uniform manifold approximation and projection (UMAP) space, (2) determination of the cluster to which each case belonged, (3) calculation for *major transitions*, and (4) construction of a directed graphical model to show *inferred pathways*.[30] A recent publication has demonstrated a severity scale of DMI based on UMAP and k-means clustering in a cross-sectional study.[23] Briefly, each eye with high-dimensional data was mapped onto the 2-dimensional UMAP space by developing the manifold, as reported by McInnes et al.[30] Subsequent clustering divided all cases into 5 grades—*Initial*, *Mild*, *Superficial*, *Moderate*, and *Severe*—based on the amounts and spatial distribution of NPSs. As we previously reported, the *Initial* group had minimal nonperfusion in both superficial and deep layers, while the *Mild* group showed a slight increase, mainly in the deep layer. The *Superficial* group had larger NPAs in the superficial layer, especially in the central 1-mm area. The *Moderate* group exhibited NPAs extending into the temporal subfield in the deep layer, and the *Severe* group showed extensive nonperfusion in both layers.[23] Each eye at baseline and the 3-year visit was embedded into this space by the calculation of Euclidean distance to 3 nearest neighbors. We then determined the severity grade to which

each eye belonged at baseline and the 3-year visit by identifying the predominant cluster among the 3 nearest points (k = 3) using the k-nearest neighbors method.

This study focused on observing cluster transitions at 3 years, defining "*major transitions*" as those from 1 grade to another involving ≥4 cases in this study. Among them, the pathways of DMI progression connecting adjacent clusters were explored to construct a directed graphical model because we hypothesized that capillary nonperfusion progresses gradually rather than continuously. We applied the following steps: (1) the determination of the starting and terminal clusters, (2) the establishment of the connections between clusters, (3) the application of conditional probability for pruning transitions, and (4) the iteration of steps 2 and 3, moving from terminal to starting clusters. First, we arranged the clusters in order according to the numbers of NPSs and determined the clusters with the least and most NPSs as the starting and terminal clusters, respectively. We then prepared the directed graph from the terminal cluster and the second one, based on the *major transitions*. When the third cluster was incorporated, 1-step or 2-step transitions were considered. We hypothesized 1-step or 2-step transitions between clusters (A→B or A→B→C) during 3 years and defined the probabilities of 2-step transitions ($P_{A\to B\to C}$) as $P_{A\to B}$ (probability of transition from cluster A to B) × $P_{B\to C}$ (probability from cluster B to C). When the sum of probabilities of possible 2-step transitions was less than the actual probabilities, we considered that the direct 1-step transition (A→C) must be present. In contrast, when the summed probabilities were greater, we rejected the 1-step transition (A→C) in this study. These processes were repeated until the starting cluster was reached. The directed arrows in the graphical model were referred to as "*inferred pathways*" of DMI progression in this study.

Statistical Analyses

All values were expressed as the median (interquartile range). Statistical significance was set at $P < 0.05$. We applied the Kruskal–Wallis test with a Bonferroni correction for continuous variables and the chi-square test for categorical variables. The statistical associations were evaluated using Spearman rank correlation coefficient. Multiple regression analysis was employed to assess the baseline factors associated with the changes in logMAR VA, using significant factors ($P < 0.05$) from univariate analyses (diabetic macular edema, central subfield thickness, and NPS counts in the deep layer). All statistical analyses were conducted using SPSS (version 24; IBM).

Results

Progression Pathway of DMI in a Longitudinal Study

We explored the NPS changes at 3 years in 151 eyes statistically (Table S1, available at www.ophthalmologyscience.org) and observed an overall increase in NPSs in both the superficial and deep layers ($P < 0.001$) (Fig 1). There are significant correlations between NPS counts at baseline and at 3 years in the superficial, deep, and both layers (Fig 1). Notably, some eyes with fewer baseline NPSs experienced significant

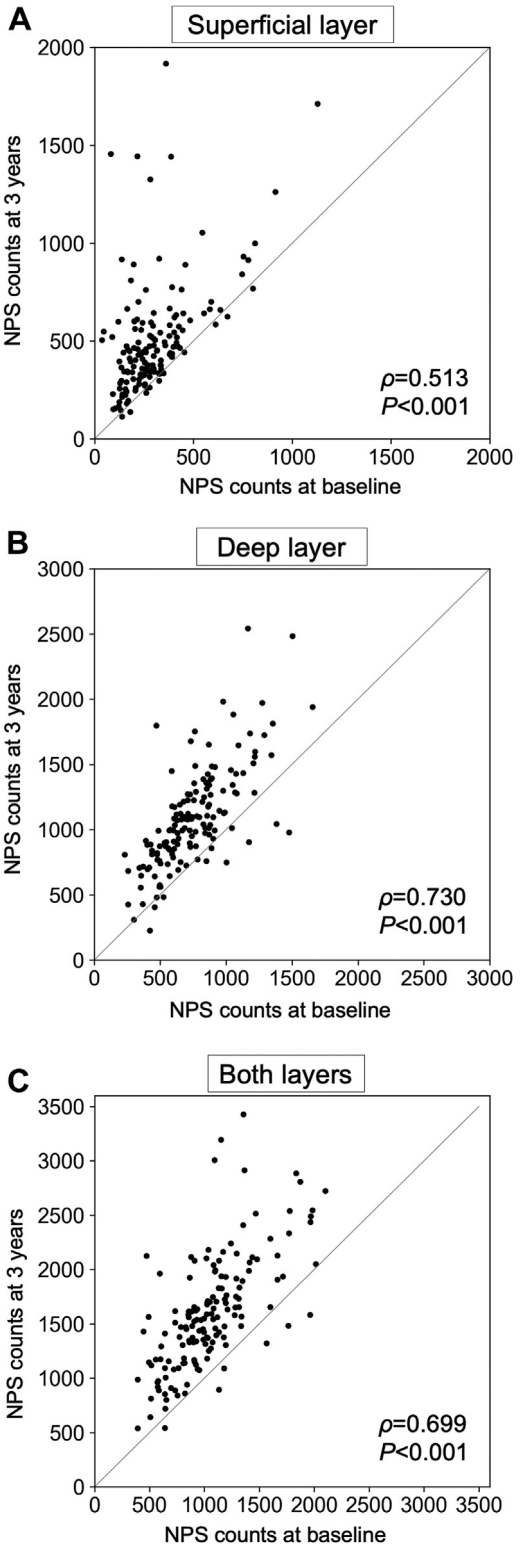

Figure 1. Nonperfusion square counts at baseline and after 3 years in all 151 eyes with diabetic retinopathy. **A,** The superficial layer. **B,** The deep layer. **C,** Both layers. NPS = nonperfusion square.

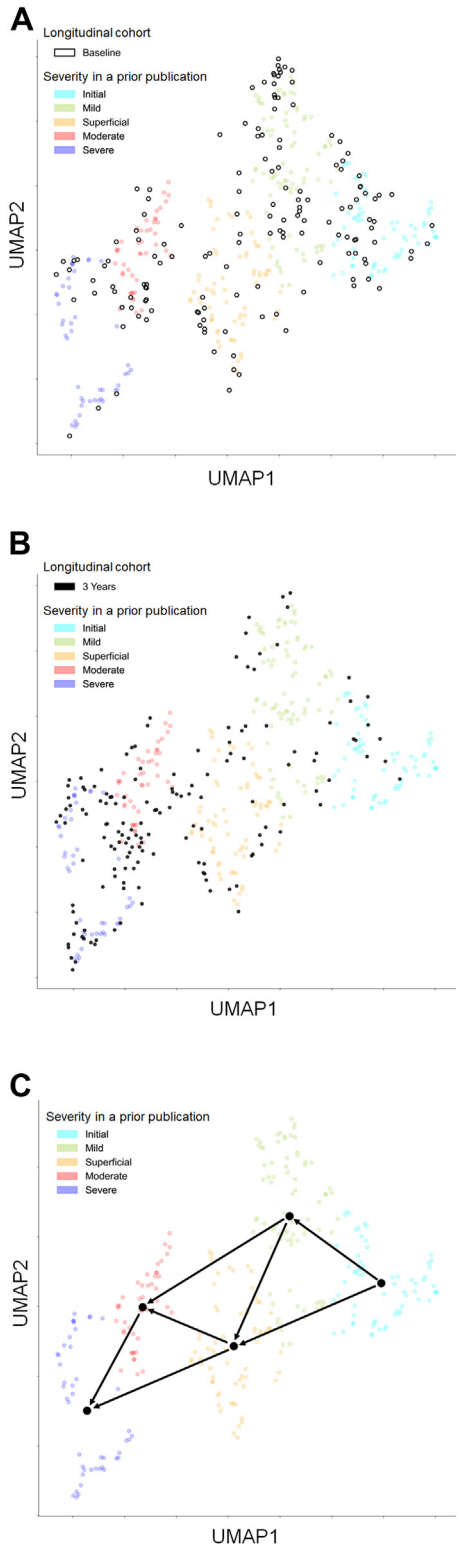

Figure 2. Embedding of all 151 eyes with diabetic retinopathy at baseline **(A)** and 3 years **(B)** onto the 2-dimensional UMAP space generated from the cross-sectional study in a prior publication.[23] Colored dots represent the dataset from the prior study, while hollow and filled black dots indicate the longitudinal cases analyzed in the current study. **A,** Eyes at baseline (hollow dots) are randomly located throughout the map. **B,** Eyes at 3 years (filled black dots) have shifted toward the left lower corner. **C,** Seven *inferred pathways* of diabetic macular ischemia progression are depicted. Arrow = *inferred pathway*; Black dot = centroid of each cluster; UMAP = uniform manifold approximation and projection.

NPS increases in the superficial layer. In the deep layer, most eyes with fewer NPSs at baseline had smaller increases in NPS counts (Fig 1).

To investigate the pathways of DMI progression, we mapped each eye at baseline and the 3-year visit onto the 2-dimensional UMAP space established in a previous publication.[23] Eyes shifted from the right upper corner to the left lower corner over time, indicating NPA deterioration and subsequent DMI progression (Fig 2A, B). Eyes with DR underwent transitions between clusters at unique frequencies (Table S2, Fig S3, available at www.ophthalmologyscience.org). Each *major transition* involved specific amounts of NPS changes (Tables 3, 4, and S5, available at www.ophthalmologyscience.org). This led us to hypothesize the main pathways of NPS progression and construct a directed graphical model (Fig 2C). Seven *inferred pathways* of DMI progression were identified: *Initial* to *Mild*, *Initial* to *Superficial*, *Mild* to *Superficial*, *Mild* to *Moderate*, *Superficial* to *Moderate*, *Superficial* to *Severe*, and *Moderate* to *Severe*.

Statistical comparisons demonstrated no significant differences in NPS changes across clusters, although specific trends were noted (Fig 4A, B). In the *Severe* group, the superficial NPS counts in the central sector remained stable, contrasting with their increases observed in the *Mild* and *Superficial* groups (Fig 4C). Eyes in the *Initial* group experienced more significant worsening in the deep NPS counts compared with those in the *Superficial* or *Moderate* groups (Fig 4D). In all parafoveal sectors, the NPS counts increased across all 5 clusters (Fig 4E, F).

Clinical Relevance of the DMI Progression Model

To evaluate the clinical relevance of our proposed model of DMI progression, we analyzed data from 103 untreated cases in a longitudinal cohort (Table S6, available at www.ophthalmologyscience.org). Visual acuity deteriorated in 46 eyes at 3 years (Fig S5, available at www.ophthalmologyscience.org). Multivariate analysis revealed no significant associations between baseline parameters and VA changes (Table S7, available at www.ophthalmologyscience.org). In contrast, worsening of logMAR VA was significantly associated with increases in parafoveal NPSs in the deep layer ($\rho = -0.291$, $P = 0.003$) (Table S8, available at www.ophthalmologyscience.org).

Certain cases within the *Superficial* group had poor logMAR VA at 3 years, but not at baseline (Fig 6A, B).[23] Notably, eyes in the *Superficial* and *Moderate* groups demonstrated more pronounced VA deterioration compared with those in the *Initial* group, suggesting that classification into these groups could serve as a predictor of future VA worsening at 3 years (Fig 6C). We further investigated VA changes during major transitions between

Table 3. Nonperfusion Square Changes in the Superficial Layer at *Major Transitions* between Clusters

	Baseline				
	Initial	*Mild*	*Superficial*	*Moderate*	*Severe*
3 yrs					
Initial	52 (6–106)	-	-	-	-
Mild	105 (64–160)	64 (42–108)	-	-	-
Superficial	276 (174–451)	183 (76–284)	141 (100–175)	-	-
Moderate	173 (45–199)	151 (87–279)	206 (187–305)	130 (59–187)	-
Severe	-	200 (144–312)	84 (65–272)	220 (110–361)	184 (96–308)

Major transition = transition with ≥4 cases.

clusters (Table S9, available at www.ophthalmologyscience.org). Transitions from the early stage (*Initial* and *Mild* groups) to the intermediate stage (*Superficial* and *Moderate* groups) were not accompanied by VA worsening. In contrast, VA deteriorated at 3 years in eyes that progressed from the *Mild*, *Superficial*, and *Moderate* groups to the *Severe* group or those that remained in the *Superficial* and *Mod*erate groups (Table 10).

Discussion

In this longitudinal study, we developed a directed graphical model to infer DMI progression pathways based on a recently reported severity scale.[23] To validate its clinical utility and investigate DMI progression over time, we established an independent cohort of 151 eyes with a 3-year follow-up. We selected this interval because preliminary data suggested that NPS changes were minimal during the first 1 or 2 years (data not shown). Further investigation regarding VA changes revealed that VA deteriorated at 3 years in the eyes of the *Superficial* and *Moderate* groups compared with those of the *Initial* group. In contrast, eyes with transition from the *Initial* or *Mild* group to the *Superficial* or *Moderate* group had no VA deterioration. These findings identify the *Superficial*, *Moderate*, and *Severe* groups as vision-threatening DMI, although future studies should elucidate the frequency of these transitions and the risk factors for progression over longer periods.

We applied a directed graphical model rather than statistical analyses to explore the clinical progression of DMI.[31–34] We then demonstrated its chronological outline: *Initial* and *Mild* as the first step without VA reduction, *Superficial* and *Moderate* as the second step, which predicts VA deterioration, and *Severe* as the third step with poor VA. Although there are no gold standards for the diagnosis and severity scales of the DMI continuum, this study suggests clinically relevant severity grades.[23] In other words, this graphical model for DMI progression might identify the *Superficial*, *Moderate*, and *Severe* groups as therapeutic targets and the *Mild* and *Moderate* groups for the preventive strategies. Despite its usefulness, we should incorporate statistical analyses in future studies to identify factors predictive of DMI progression or VA deterioration.

The comparisons of NPS counts between baseline and 3 years suggest the progression of DMI, which is consistent with rare transitions to less severe groups. We therefore constructed the directed graphical model to interpret DMI progression concisely, compared to the stepwise severity grades based on the FAZ morphologies on fluorescein angiography images.[31] The graphical model elucidated 2 main pathways during the intermediate stages: *Superficial* and *Moderate*. The presence of these 2 distinct pathways may explain the different phenotypes of DMI.[1] The superficial vascular plexus primarily supplies the inner retina, and its ischemia has been linked to damages in the retinal nerve fiber layer and ganglion cell layer.[35] In contrast, the deep capillary plexuses, which supply the outer retina and photoreceptors, are more closely associated with ellipsoid zone disruption and photoreceptor degeneration.[36] Future studies should elucidate the functional and morphological biomarkers of neurodegeneration in each group and the processes of neurovascular degeneration leading to the *Severe* group.

Table 4. Nonperfusion Square Changes in the Deep Layer at *Major Transitions* between Clusters

	Baseline				
	Initial	*Mild*	*Superficial*	*Moderate*	*Severe*
3 yrs					
Initial	60 (−5 to 176)	-	-	-	-
Mild	293 (268–345)	66 (56–97)	-	-	-
Superficial	442 (364–488)	270 (181–306)	149 (97–172)	-	-
Moderate	389 (365–518)	398 (311–496)	396 (364–418)	321 (235–482)	-
Severe	-	479 (417–783)	538 (386–662)	400 (315–568)	314 (243–412)

Major transition = transition with ≥4 cases.

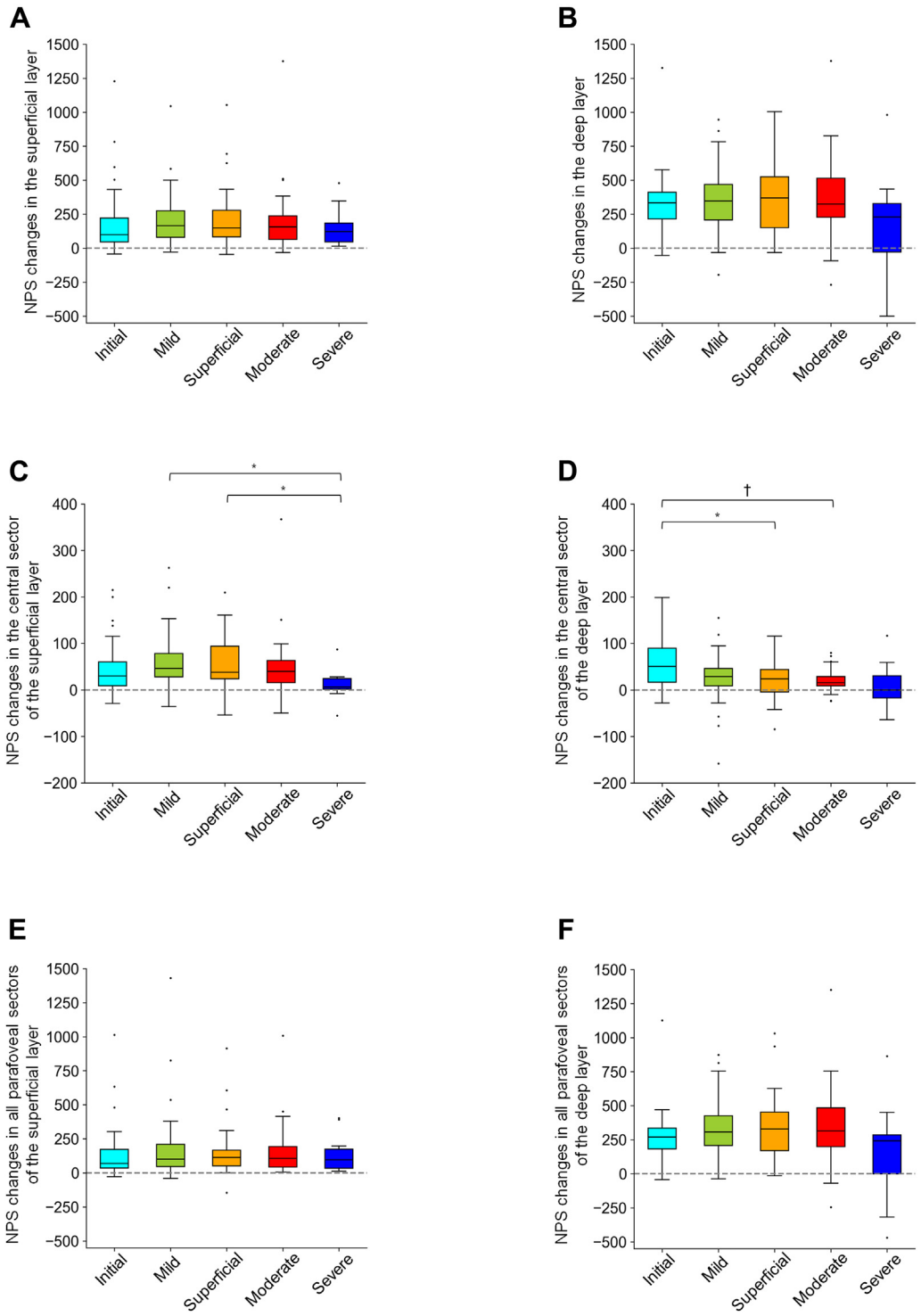

Figure 4. Nonperfusion square changes in each cluster of all 151 eyes with diabetic retinopathy. All sectors **(A, B)**. The central sector **(C, D)**. All parafoveal sectors **(E, F)**. The superficial **(A, C, E)** and deep **(B, D, F)** layers. *$P < 0.05$; †$P < 0.01$. NPS = nonperfusion square.

Visual acuity reduction is generally associated with a decrease in the perfusion metrics or an increase in the nonperfusion metrics in DR, in accordance with previous publications.[4–9,37] In this study, VA deteriorated during the transition from the *Mild*, *Superficial*, and *Moderate* groups to the *Severe* group. We speculate that malnutrition and hypoxia within the NPAs irreversibly contribute to visual disturbance during the *Superficial* and *Moderate* stages of transitions to the *Severe* stage. These stages may share common pathological mechanisms, leading to concurrent degenerative

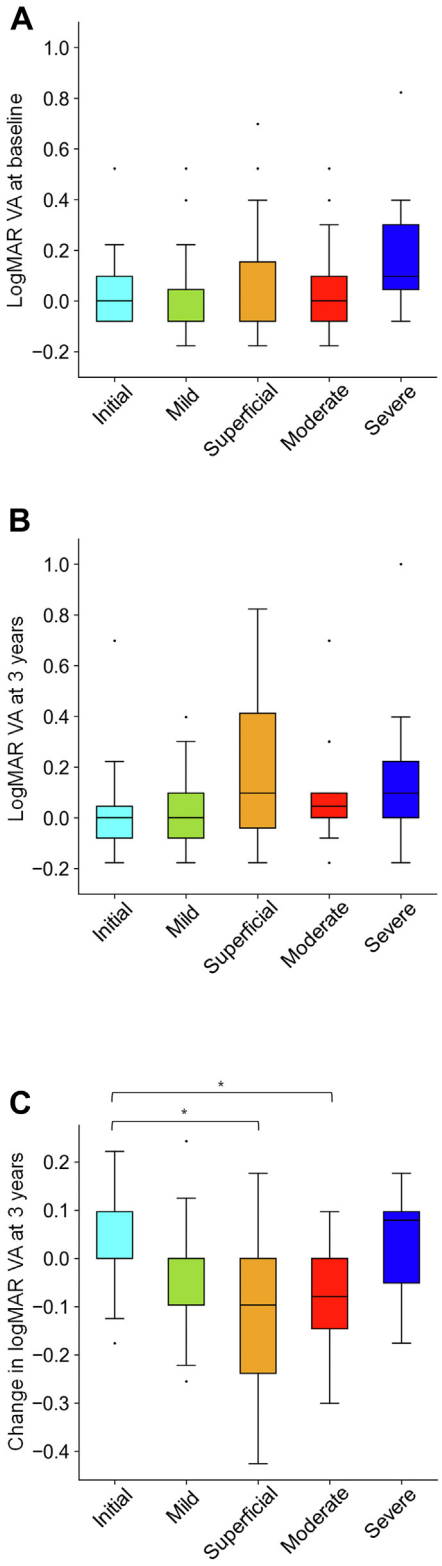

Figure 6. Comparisons of logMAR VA across clusters in all 103 untreated eyes with diabetic retinopathy. LogMAR **(A)** at baseline and **(B)** at 3 years. **C,** Change in logMAR at 3 years. *$P < 0.01$. logMAR = logarithm of the minimum angle of resolution; VA = visual acuity.

processes in both neurons and vessels.[38] Neurotoxic factors might be released from or passed through vascular endothelial cells, continuing until the complete loss of vascular cells terminates the neurodegenerative processes.[39] Vice versa, neurodegeneration in the inner retinal layers might lead to loss of angiogenic factors and subsequent capillary obstruction.[40,41] Multivariate analysis showed that baseline NPS counts across all untreated eyes were not significantly associated with VA changes. In contrast, the graphical model based on the DMI severity scale revealed more pronounced VA deterioration during the intermediate stages, emphasizing the importance of a stage-specific approach in understanding DMI progression and its impact on visual function.

Visual acuity was not deteriorated at the transitions from the *Initial* or *Mild* groups to the *Superficial* and *Moderate* groups, despite aggravating capillary nonperfusion. It is consistent with no differences in VA between the *Initial*, *Mild*, *Superficial*, and *Moderate* groups in a cross-sectional study.[23] We hypothesized 2 possible explanations: the threshold of nutritional deficiency for retinal function and different mechanisms underpinning capillary nonperfusion with and without visual dysfunction. Retinas are redundantly nourished by retinal arteries and the choroidal vessels, so mild reduction of retinal capillaries might not influence the function of retinal neurons.[8] As another perspective, we should consider that transient and permanent capillary occlusion reduces the flow signals on OCTA images. Blood cells, e.g., leukocytes, erythrocytes, and platelets, could induce transient plugging of capillary lumen, whereas neurovascular degeneration might aggravate cell death in vascular cells and permanent occlusion with extracellular matrix.[42,43]

There are several limitations to this study. The single-center design with the inclusion and exclusion criteria may result in selection bias. In particular, several artifacts at the acquisition and creation of OCTA images may influence the quantitative analyses.[44] The use of a specific SS-OCTA device and image processing methods may limit the generalizability of our findings. We selected NPSs as a nonperfusion metric, although we have to validate the consistency with other perfusion and nonperfusion metrics.[1] Multicenter studies incorporating independent cohorts, diverse imaging technologies, and analytical algorithms will be necessary to validate and expand upon our results. We selected the UMAP for dimensionality reduction and better visualization of the data space, although future studies should confirm the reproducibility by other methods to reduce dimensionality.[30,45] In our prior study, the *Superficial* and *Moderate* groups were classified as distinct based on objective clustering.[23] However, given their shared status as intermediate stages in DMI progression, future studies may refine or even merge these groups based on additional data. Our directed graphical model considered 1-step and 2-step transitions but not 3-step transitions between clusters because the inferred probabilities of transitions were not consistent with the actual probabilities. When 3-step transitions were included, the discrepancy between actual and estimated probabilities

Table 10. Logarithm of the Minimum Angle of Resolution Visual Acuity Changes at *Major Transitions* between Clusters in Untreated 103 Eyes

	Baseline				
	Initial	*Mild*	*Superficial*	*Moderate*	*Severe*
3 yrs					
Initial	0.023 (0.000–0.084)	-	-	-	-
Mild	0.000 (0.000–0.059)	-	-	-	-
Superficial	0.103 (0.073–0.109)	0.000 (−0.040 to 0.091)	−0.097 (−0.368 to 0.000)	-	-
Moderate	-	0.000 (−0.097 to 0.000)	0.000 (−0.125 to 0.000)	−0.079 (−0.125 to −0.046)	-
Severe	-	−0.097 (−0.137 to −0.023)	−0.125 (−0.207 to −0.073)	−0.051 (−0.176 to 0.000)	−0.026 (−0.145 to 0.059)

Major transition = transition with ≥4 cases.

increased (data not shown), suggesting that 3-step transitions are less likely to occur within a 3-year period. This could be further clarified through more frequent acquisitions of OCTA images in future studies. While our focus on major transitions provided valuable insights into the most clinically relevant changes, further investigation into the characteristics of eyes with minor transitions is warranted.

In conclusion, this longitudinal study validates the use of a novel classification system for DMI on OCTA images and introduces a directed graphical model for understanding its progression. These findings contribute to the ongoing effort to establish reliable diagnostic and staging criteria for DMI, with the ultimate goal of improving patient outcomes through timely and targeted interventions.

Footnotes and Disclosures

Originally received: November 5, 2024.
Final revision: February 19, 2025.
Accepted: March 4, 2025.
Available online: March 12, 2025. Manuscript no. XOPS-D-24-00483.

Department of Ophthalmology and Visual Sciences, Kyoto University Graduate School of Medicine, Kyoto, Japan.

Disclosure(s):

All authors have completed and submitted the ICMJE disclosures form.

The authors made the following disclosures:

T.M.: Grants − Novartis Pharma; Royalties − Bayer Yakuhin, Santen Pharmaceutical, Kowa Pharmaceutical, Chugai Pharmaceutical, Novartis Pharma, Senju Pharmaceutical, Johnson & Johnson K.K., Mitsubishi Tanabe Pharma.

A.T.: Grants − Canon, Santen Pharmaceutical, Otsuka Pharmaceutical, Alcon Japan, Wakamoto Pharmaceutical, AMO Japan, Findex, Sumitomo Pharma, Senju Pharmaceutical, Bayer Yakuhin, Chugai Pharmaceutical, ROHTO NITTEN; Royalties − Santen Pharmaceutical, Senju Pharmaceutical, Novartis Pharma, Otsuka Pharmaceutical, Wakamoto Pharmaceutical, MSD, HOYA, Johnson & Johnson K.K., NIKON SOLUTIONS, Bayer Yakuhin, Chugai Pharmaceutical, Alcon Japan, AMO Japan, Kowa Company, Ellex, Canon, ROHTO Pharmaceutical; Consultant − Senju Pharmaceutical, Chugai Pharmaceutical, HOYA, Sumitomo Pharma, Alcon Japan, Boehringer Ingelheim, Bayer Yakuhin, Janssen Pharmaceutical, KYOWA KIRIN.

This study was funded by a Grant-in-Aid for Scientific Research of the Japan Society for the Promotion of Science (grant number: 23K09004). The funding organization had no role in the design or conduct of this research.

HUMAN SUBJECTS: Human subjects were included in this study. This study was approved by the Kyoto University Graduate School and Faculty of Medicine Ethics Committee and adhered to the tenets of the Declaration of Helsinki. Written informed consent was obtained from all participants before inclusion in the study.

No animal subjects were used in this study.

Author Contributions:

Conception and design: Yoshida, Murakami

Data collection: Yoshida, Murakami, Nishikawa, Ishihara, Mori, Tsujikawa

Analysis and interpretation: Yoshida, Murakami, Tsujikawa

Obtained funding: Murakami

Overall responsibility: Yoshida, Murakami

Abbreviations and Acronyms:
DMI = diabetic macular ischemia; **DR** = diabetic retinopathy; **FAZ** = foveal avascular zone; **logMAR** = logarithm of the minimum angle of resolution; **NPA** = nonperfusion area; **NPS** = nonperfusion square; **OCTA** = OCT angiography; **SS** = swept-source; **UMAP** = uniform manifold approximation and projection; **VA** = visual acuity.

Keywords:
Diabetic macular ischemia, Nonperfusion areas, Semiautomatic quantification, OCT angiography, Uniform manifold approximation and projection.

Correspondence:
Tomoaki Murakami, MD, PhD, Department of Ophthalmology and Visual Sciences, Kyoto University Graduate School of Medicine, 54 Shougoin Kawahara-cho, Sakyo-ku, Kyoto 606-8507, Japan. E-mail: mutomo@kuhp.kyoto-u.ac.jp.

References

1. Cheung CMG, Fawzi A, Teo KY, et al. Diabetic macular ischaemia- a new therapeutic target? *Prog Retin Eye Res*. 2022;89:101033.
2. Waheed NK, Rosen RB, Jia Y, et al. Optical coherence tomography angiography in diabetic retinopathy. *Prog Retin Eye Res*. 2023;97:101206.

3. Dollery CT, Bulpitt CJ, Kohner EM. Oxygen supply to the retina from the retinal and choroidal circulations at normal and increased arterial oxygen tensions. *Invest Ophthalmol*. 1969;8:588−594.
4. Sim DA, Keane PA, Zarranz-Ventura J, et al. The effects of macular ischemia on visual acuity in diabetic retinopathy. *Invest Ophthalmol Vis Sci*. 2013;54:2353−2360.
5. Balaratnasingam C, Inoue M, Ahn S, et al. Visual acuity is correlated with the area of the foveal avascular zone in diabetic retinopathy and retinal vein occlusion. *Ophthalmology*. 2016;123:2352−2367.
6. Samara WA, Shahlaee A, Adam MK, et al. Quantification of diabetic macular ischemia using optical coherence tomography angiography and its relationship with visual acuity. *Ophthalmology*. 2017;124:235−244.
7. Tsai ASH, Gan ATL, Ting DSW, et al. Diabetic macular ischemia: correlation of retinal vasculature changes by optical coherence tomography angiography and functional deficit. *Retina*. 2020;40:2184−2190.
8. Terada N, Murakami T, Ishihara K, et al. Clinical relevance of parafoveal intercapillary spaces and foveal avascular zone in diabetic retinopathy without macular edema. *Invest Ophthalmol Vis Sci*. 2022;63:4.
9. Yang D, Tang Z, Ran A, et al. Assessment of parafoveal diabetic macular ischemia on optical coherence tomography angiography images to predict diabetic retinal disease progression and visual acuity deterioration. *JAMA Ophthalmol*. 2023;141:641−649.
10. Arima M, Nakao S, Kaizu Y, et al. Diabetic vascular hyperpermeability: optical coherence tomography angiography and functional loss assessments of relationships among retinal vasculature changes. *Sci Rep*. 2021;11:4185.
11. Tsai WS, Thottarath S, Gurudas S, et al. Topographic correlation of microperimetry with structural characteristics in diabetic macular ischemia. *Am J Ophthalmol*. 2024;257:25−33.
12. Spaide RF. Volume-rendered angiographic and structural optical coherence tomography. *Retina*. 2015;35:2181−2187.
13. Dodo Y, Murakami T, Suzuma K, et al. Diabetic neuroglial changes in the superficial and deep nonperfused areas on optical coherence tomography angiography. *Invest Ophthalmol Vis Sci*. 2017;58:5870−5879.
14. Tsai WS, Thottarath S, Gurudas S, et al. Characterization of the structural and functional alteration in eyes with diabetic macular ischemia. *Ophthalmol Retina*. 2023;7:142−152.
15. Aiello LP, Bursell SE, Clermont A, et al. Vascular endothelial growth factor−induced retinal permeability is mediated by protein kinase C in vivo and suppressed by an orally effective β-isoform−selective inhibitor. *Diabetes*. 1997;46:1473−1480.
16. Lee J, Moon BG, Cho AR, Yoon YH. Optical coherence tomography angiography of DME and its association with anti-VEGF treatment response. *Ophthalmology*. 2016;123:2368−2375.
17. Scarinci F, Nesper PL, Fawzi AA. Deep retinal capillary nonperfusion is associated with photoreceptor disruption in diabetic macular ischemia. *Am J Ophthalmol*. 2016;168:129−138.
18. Snodderly DM, Weinhaus RS, Chopb JC. Neural-vascular relationships in central retina of macaque monkeys (Macaca fascicularis). *J Neurosci*. 1992;12:1169−1193.
19. Balaratnasingam C, An D, Freund KB, et al. Correlation between histologic and OCT angiography analysis of macular circulation. *Ophthalmology*. 2019;126:1588−1589.
20. Spaide RF, Klancnik JM, Cooney MJ. Retinal vascular layers imaged by fluorescein angiography and optical coherence tomography angiography. *JAMA Ophthalmol*. 2015;133:45−50.
21. Jia Y, Tan O, Tokayer J, et al. Split-spectrum amplitude-decorrelation angiography with optical coherence tomography. *Opt Express*. 2012;20:4710−4725.
22. Choi W, Moult EM, Waheed NK, et al. Ultrahigh-speed, swept-source optical coherence tomography angiography in nonexudative age-related macular degeneration with geographic atrophy. *Ophthalmology*. 2015;122:2532−2544.
23. Yoshida M, Murakami T, Nishikawa K, et al. Severity scale of diabetic macular ischemia based on the distribution of capillary nonperfusion in OCT angiography. *Ophthalmol Sci*. 2024;5:100603.
24. Durbin MK, An L, Shemonski ND, et al. Quantification of retinal microvascular density in optical coherence tomographic angiography images in diabetic retinopathy. *JAMA Ophthalmol*. 2017;135:370−376.
25. Uchitomi D, Murakami T, Dodo Y, et al. Disproportion of lamellar capillary non-perfusion in proliferative diabetic retinopathy on optical coherence tomography angiography. *Br J Ophthalmol*. 2020;104:857−862.
26. Wilkinson CP, Ferris FL, Klein RE, et al. Proposed international clinical diabetic retinopathy and diabetic macular edema disease severity scales. *Ophthalmology*. 2003;110:1677−1682.
27. Chalam KV, Bressler SB, Edwards AR, et al. Retinal thickness in people with diabetes and minimal or no diabetic retinopathy: Heidelberg spectralis optical coherence tomography. *Invest Ophthalmol Vis Sci*. 2012;53:8154−8161.
28. Terada N, Murakami T, Ishihara K, et al. Quantification of dilated deep capillaries in diabetic retinopathy on optical coherence tomography angiography. *Sci Rep*. 2023;13:17884.
29. Canny J. A computational approach to edge detection. *IEEE Trans Pattern Anal Mach Intell*. 1986;8:679−698.
30. McInnes L, Healy J, Melville J. Uniform manifold approximation and projection for dimension reduction. *arXiv*. 2018. https://doi.org/10.48550/arXiv.1802.03426.
31. Sim DA, Keane PA, Zarranz-Ventura J, et al. Predictive factors for the progression of diabetic macular ischemia. *Am J Ophthalmol*. 2013;156:684−692.
32. Sun Z, Tang F, Wong R, et al. OCT angiography metrics predict progression of diabetic retinopathy and development of diabetic macular edema. *Ophthalmology*. 2019;126:1675−1684.
33. Ribeiro L, Marques IP, Santos T, et al. Characterization of 2-year progression of different phenotypes of nonproliferative diabetic retinopathy. *Ophthalmic Res*. 2023;66:228−237.
34. Ong JX, Konopek N, Fukuyama H, Fawzi AA. Deep capillary nonperfusion on OCT angiography predicts complications in eyes with referable nonproliferative diabetic retinopathy. *Ophthalmol Retina*. 2023;7:14−23.
35. Dupas B, Minvielle W, Bonnin S, et al. Association between vessel density and visual acuity in patients with diabetic retinopathy and poorly controlled type 1 diabetes. *JAMA Ophthalmol*. 2018;136:721−728.
36. Bhardwaj S, Tsui E, Zahid S, et al. Value of fractal analysis of optical coherence tomography angiography in various stages of diabetic retinopathy. *Retina*. 2018;38:1816−1823.
37. Cheung CMG, Pearce E, Fenner B, et al. Looking ahead: visual and anatomical endpoints in future trials of diabetic macular ischemia. *Ophthalmologica*. 2021;244:451−464.
38. Joussen AM, Poulaki V, Mitsiades N, et al. Nonsteroidal anti-inflammatory drugs prevent early diabetic retinopathy via TNF-alpha suppression. *FASEB J*. 2002;16:438−440.
39. Sofroniew MV. Astrocyte barriers to neurotoxic inflammation. *Nat Rev Neurosci*. 2015;16:249−263.

40. Kim I, Ryan AM, Rohan R, et al. Constitutive expression of VEGF, VEGFR-1, and VEGFR-2 in normal eyes. *Invest Ophthalmol Vis Sci*. 1999;40:2115–2121.
41. Lee S, Chen TT, Barber CL, et al. Autocrine VEGF signaling is required for vascular homeostasis. *Cell*. 2007;130:691–703.
42. Miyamoto K, Amer Khosrof S, Bursell SE, et al. Prevention of leukostasis and vascular leakage in streptozotocin-induced diabetic retinopathy via intercellular adhesion molecule-1 inhibition. *Proc Natl Acad Sci U S A*. 1999;96:10836–10841.
43. Powner MB, Sim DA, Zhu M, et al. Evaluation of nonperfused retinal vessels in ischemic retinopathy. *Invest Ophthalmol Vis Sci*. 2016;57:5031–5037.
44. Spaide RF, Fujimoto JG, Waheed NK. Image artifacts in optical coherence tomography angiography. *Retina*. 2015;35:2163–2180.
45. Van Der Maaten L, Hinton G. Visualizing data using T-SNE. *J Mach Learn Res*. 2008;9:2579–2605.